CONF-930202--6

MICROSTRUCTURE AND ASSOCIATED PROPERTIES OF $YBa_2Cu_3O_x$ SUPERCONDUCTORS PREPARED BY MELT-PROCESSING TECHNIQUES*

U. Balachandran, W. Zhong, C. A. Youngdahl, and R. B. Poeppel
Materials and Components Technology Division
Argonne National Laboratory
Argonne, IL 60439

ANL/MCT/CP--76965

DE93 010675

March 1993

DISCLAIMER

INVITED paper submitted for publication in the Proceedings of the 1993 TMS Annual Meeting, Symposium on High Temperature Superconductors, Denver, CO, February 21-25, 1993.

*Work supported by the U.S. Department of Energy (DOE), Conservation and Renewable Energy, as part of a DOE program to develop electric power technology, under Contract W-31-109-ENG-38.

MICROSTRUCTURE AND ASSOCIATED PROPERTIES OF $YBa_2Cu_3O_x$ SUPERCONDUCTORS PREPARED BY MELT PROCESSING TECHNIQUES

U. Balachandran, W. Zhong, C. A. Youngdahl, and R. B. Poeppel
Materials and Components Technology Division
Argonne National Laboratory
Argonne, IL 60439

ABSTRACT

From the standpoint of applications, melt-processed bulk $YBa_2Cu_3O_x$ (YBCO) superconductors are of considerable interest. We have studied the microstructure and levitation force of melt-processed YBCO, YBCO plus Y_2BaCuO_5, and YBCO plus Pt samples. Large single crystalline samples, grown using a seeding technique, were also studied. The levitation force is highest in melt-processed samples made by the seeding technique.

INTRODUCTION

Since the discovery of the $YBa_2Cu_3O_x$ (YBCO) superconductor, tremendous efforts have been made to apply this material for practical use. Most applications have been hindered by low transport critical current density (J_c), especially in presence of a magnetic field [1]. Various processing techniques have been developed to improve the J_c. Particularly successful are the melt-processing technique developed by Jin et al. [2] for YBCO and the subsequent variations adapted by several other groups [3–5]. Melt-processed YBCO has been found to have high J_c (>10^4 A/cm^2 at 77K and 1T) values [3, 4, 6–8]. Improvements in J_c are due to large grains aligned along the crystallographic c-axis and enhanced flux pinning properties of individual grains. The large

increase in J_c obtained in melt-processed samples brings YBCO one step closer to practical applications. Superconductor/permanent magnet bearings, flywheels for energy storage, high field magnets, and magnetic shields are some of the potential applications of the melt-processed bulk YBCO superconductors.

The exact mechanism of enhanced flux pinning in melt-processed samples is the subject of many investigations [9–12]. Fine precipitates of Y_2BaCuO_5 (211) are considered as potential flux pinning sites by many groups [12–14]. 211 precipitates are always present in melt-processed YBCO due to incomplete peritectic reaction. The morphology of 211 particles is important [15], and second phase additions which affect the 211 morphology and size are of considerable interest. Several groups have reported the refinement of 211 precipitates through Pt additions [16–20]. Varanasi and McGinn [20] found that the 211 precipitates segregate and form tracks in melt-textured PtO_2–doped YBCO samples. In this paper, we melt-processed YBCO, YBCO + 211, and YBCO + Pt. The microstructure and levitation force are characterized for these samples and the results are presented here.

EXPERIMENTAL

Stoichiometeric YBCO powder was prepared by reduced-pressure calcination of Y_2O_3, $BaCO_3$, and CuO in flowing oxygen at a pressure of ≈2 mm Hg [21]. Fine agglomerates of 211, obtained form a commercial source, were mixed into YBCO in the amount 6–80 mol.%. For the experiments with Pt addition, 0.5 wt.% of fine Pt powder was mixed with YBCO using a mortar and pestle. Pellets (≈4.5 cm diameter, ≈0.6 cm thick) of YBCO, YBCO + 211 and

YBCO + Pt were compacted by uniaxial pressing at room temperature. These pellets were rapidly heated to ≈1070°C, slowly cooled (≈1°C/h) to ≈970°C and then cooled at ≈60°C/h to room temperature. These melt-processed samples were oxygen annealed for ≈200 h at 500°C. The microstructures of the three sets of samples were examined by optical microscopy. The levitation forces were measured on a triple beam balance (Figure 1). A small rare-earth permanent magnet (13.3 mm dia.; 5 mm thick; ≈2.8 KGauss field strength) was attached to a glass beaker and placed on the pan of the balance. The superconductor sample was placed in a non-magnetic container and supported by a vertical laboratory stand. The deflection of the pointer of the balance was correlated to the force on the magnet. The levitation force as a function of height was then determined by moving the magnet toward the superconductor and monitoring the beam deflection.

RESULTS AND DISCUSSION

At the melt-processing temperature of ≈1070°C, the YBCO sample consists of a liquid phase plus 211 particles. As the temperature is lowered, the reaction between the liquid phase and 211 lead to nucleation and growth of 123 crystals. This process consumes most of the 211 phase; however, some of the 211 phase becomes trapped before it is consumed, which accounts for the presence of 211 in the melt-processed stoichiometeric YBCO as shown in Fig. 2(a).

Figures 2(b) and (c) show the optical micrograph of melt-processed YBCO + 211 and YBCO + Pt. As seen from these micrographs (Fig. 2(a) and (b)), the 211 particles in YBCO and YBCO + 211 are spherical with size range 2–15 μm.

The 211 in YBCO + Pt sample, in contrast, are generally acicular in shape with lengths upto ≈30 μm and widths as small as ≈2 μm.

High-resolution transmission electron microscopy revealed very fine precipitates (≈0.1 μm) of 211 in all of the samples studied in this investigation. The relative amounts of 211 in YBCO are, as expected, higher in YBCO + 211 than those observed in melt-processed stoichiometeric YBCO. In both cases, the size and distribution of the 211 are similar. The reduction in the size of 211 in YBCO + Pt samples (Fig.2c) is due to a reduction in surface energy between 211 and the melt and/or changes in chemical potential gradients as previously suggested by Izumi, et al. [22]. Varanasi and McGinn [20] observed acicular 211 precipitates in melt-processed YBCO with PtO_2 addition. They are thought to be a manifestation of a decrease in the surface energy of 211 particles in the melt as a result of PtO_2 addition. The acicular 211 precipitates observed in the present study in melt-processed YBCO + Pt are consistent with the earlier results [20, 22].

The measured levitation force vs. distance between superconductor and the permanent magnet is shown in Figure 3 for melt-processed YBCO, YBCO + 211, and YBCO sample sintered at ≈950°C (solid-state sintering). The repulsive force is increased as the 2.8 kGauss magnet is moved toward the superconductor and reaches ≈60 gm at 1-5mm gap for melt-processed YBCO; ≈72 gm for melt-processed YBCO + 211; and ≈12 gm for solid-state sintered YBCO. When the magnet is moved away from the superconductor, the repulsive force decreased rapidly and at a certain distance, the force becomes attractive, indicating that some magnetic fields are trapped by the superconductors. The attractive force will be increased if the trapped field is increased. As seen from Fig. 3, a systematic increase in levitation force is

observed as we progress form the solid state sintered YBCO to melt-processed YBCO and YBCO + 211. Stronger force is observed in the YBCO + 211 than in the melt-processed YBCO samples. The increase in levitation force in melt-processed samples is the result of improved flux pinning due to precipitates. Even though the dimension of the 211 precipitates in melt-processed samples are much larger than the coherence length of the superconductor, flux pinning could still be effective, possibly due to defects such as stacking faults, strain fields, etc., at or near the interface between the 211 precipitates and the YBCO matrix and/or cation nonstoichiometry at the interfaces.

The attractive force increases (Fig. 3) from solid-state sintered to melt-processed YBCO to melt-processed YBCO + 211. The attractive force, as mentioned earlier, is due to magnetic field trapped by the superconductors. In zero-field cooled experiment using a rare-earth magnet with average field strength ≈2.8 kG, we measured the trapped field to be ≈16 G, ≈220 G, and ≈240 G in solid state sintered YBCO, melt-processed YBCO and YBCO + 211, respectively. The attractive force shown in Fig. 3 is consistent with measured trapped-fields in these three samples.

Large crystals (domain) of YBCO are formed when melt-processing of YBCO + Pt was done with a small (≈1 mm size) $SmBa_2Cu_3O_x$ (Sm-123) single crystal seed. Domains up to ≈3 cm in diameter, as shown in Fig. 4, were grown using the seeding technique. Murakami, et al.[23] and Blohowiak, et al. [24] have grown large, oriented grains of YBCO using Sm-123 seeds in their quench-melt-growth-processed (QMGP) samples. In QMGP, the YBCO is melted at temperature ≈1450°C, quenched, and the resulting material is ground, compacted and then melt-processed using heating and cooling schedules followed in the present study. Large single crystals of YBCO grown

by QMGP using Sm–123 seed has shown high J_c and trapped fields. The 211 precipitates are acicular in shape with lengths upto ≈30 μm and widths as small as ≈2 μm. In addition to these large precipitates, smaller size precipitates on the order of ≈1 μm is distributed inhomogeneously along tracks as shown in Fig. 5. Varanasi and McGinn [20] also observed such tracks of 211 particles in PtO_2 doped YBCO and attributed it to pushing of the fine 211 particles by the growth front propagating across the crystal face during formation of the YBCO crystals.

The levitation force measured in samples prepared using Sm–123 seed is shown in Figure 6. The force is ≈210 gm at a gap of 1.5 mm between the superconductor and permanent magnet. For comparison, the force in melt–processed YBCO + 211 is only 72 g. The increase in levitation force in melt–processed YBCO with Sm–123 seed is due t formation of large crystals with controlled orientation and improved flux pinning. Blohowiak et al. [24] observed fine nanometer sized 211 precipitates, planar defects, and strain contrasts in melt–processed YBCO using Sm–123 seed. All these defects may be responsible for the observed high levitation force. The trapped field in our samples are in the range 450–600 G and resulted in observed larger attractive force.

CONCLUSION

Melt–processing of YBCO with Pt resulted in acicular 211 precipitates whereas samples with no Pt addition exhibited large spherical 211 precipitates. Pt addition caused segregation of 211 particles along certain tracks. This is due to pushing of the fine 211 particles by the growth front

propagating across the crystal face during formation of the YBCO crystals. Large single crystals of YBCO were grown using Sm–123 crystals as seed during melt–processing YBCO with Pt addition. These samples showed very high levitation force and high flux trapping.

ACKNOWLEDGEMENT

This work was supported by the U.S. Department of Energy, Conservation and Renewable Energy, as part of a program to develop electric power technology, under Contract W–31–109–Eng–38. UB gratefully acknowledges several helpful discussions with Prof. Paul McGinn, University of Notre Dame. The authors thank Dr. M. Strasik and Dr. K. Y. Blohowiak of Boeing Corp. for providing the Sm–123 single crystal seeds.

REFERENCES

1. S. Jin, R. C. Sherwood, T. H. Tiefel, R. B. VanDover, D. W. Johnson, Jr., and G. S. Grader, Appl. Phys. Lett. **51** (1987) 855.

2. S. Jin, R. C. Sherwood, T. H. Tiefel, R. B. VanDover, and D. W. Johnson, Jr., Appl. Phys. Lett. **51** (1987) 203.

3. M. Murakami, M. Morita, K. Doi, and K. Miyamoto, Jpn. J. Appl. Phys. **28** (1989) 1189.

4. K. Salama, V. Selvamanickam, L. Gao, and K. Sun, Appl. Phys. Lett. **54** (1989) 2352.

5. M. Murakami, S. Gotoh, N. Koshizuka, S. Tanaka, T. Matsushita, S. Kambe, K. Kitazawa, Cryogenics **30** (1990) 390.

6. P. J. McGinn, W. Chen, N. Zhu, U. Balachandran, and M. T. Lanagan, Physica C **165** (1990) 480.

7. S. Kuharuangrong and J. Taylor, J. Am. Cerm. Soc., **74** (1991) 1964.

8. D. Shi, M. M. Fang, J. Akujieze, M. Xu, J. G. Chen, and C. Segre, Appl. Phys. Lett. **57** (1990) 2606.

9. P. J. McGinn, N. Zhu, W. Chen, S. Sengupta, and T. Li, Physica C **176** (1991) 203.

10. S. Jin, G. W. Kammlott, T. H. Tiefel, T. T. Kodas, T. L. Ward, and D. M. Kroeger, Physica C **181** (1991) 57.

11. A. K. Gangopadhyay, U. Balachandran, and R. B. Poeppel, Physica C **201** (1992) 6.

12. S. Sengupta, D. Shi, Z. Wang, A. C. Biondo, U. Balachandran, and K. C. Goretta, Physica C **199** (1992) 43.

13. D. F. Lee, V. Selvamanickam, and K. Salama, Physica C **202** (1992) 83.

14. M. Murakami, K. Yamaguchi, H. Fujimoto, N. Nakamura, T. Taguchi, N. Koshizuka, and S. Tanaka, Cryogenics **32** (1992) 930.

15. Z. L. Wang, A. Goyal, and D. M. Kroeger, Phys. Rev. B (in press).

16. N. Ogawa, I. Hirabayashi, and S. Tanaka, Physica C **177** (1991) 101.

17. N. Ogawa, M. Yoshida, I. Hirabayashi, and S. Tanaka, Supercon. Sci. Technol. **5** (1992) 589.

18. S. Gauss, S. Elschner, and H. Bestgen, Cryogenics **32** (1992) 965.

19. M. Morita, M. Tanaka, S. Takebayashi, K. Kimura, K. Miyamoto, and K. Sawano, Jap. J. App. Phys. **30** (1991) L813.

20. C. Varanasi and P. J. McGinn, Submitted to Physica C.

21. U. Balachandran, R. B. Poeppel, J. E. Emerson, S. A. Johnson, M. T. Lanagan, C. A. Youngdahl, K. C. Goretta, and N. G. Eror, Mater. Lett. **8** (1989) 454.

22. T. Izumi, Y. Nakamura, T. H. Sung, and Y. Shiohara, J. Mater. Res. **7** (1992) 801.

23. M. Murakami, T. Oyama, H. Fujimoto, T. Taguchi, S. Gotoh, Y. Shiohara, N. Koshizuka, and S. Tanaka, Jap. J. Appl. Phys. **29** (1990) L1991.

24. K. Y. Blohowiak, D. F. Garrigus, T. S. Luhman, K. E. McCrary, M. Strasik, I. A. Aksay, F. Dogan, W. B. Hicks, J. Liu, and M. Sarikaya, To be published in proceedings of 1992 Applied Superconductivity Conference, Chicago, IL, August 23–28, 1992.

FIGURE CAPTIONS

Figure 1: Apparatus for levitation force measurement.

Figure 2: Optical micrograph of melt-processed (a) stoichiometric YBCO; (b) YBCO + 211; and (c) YBCO + Pt.

Figure 3: Levitation force vs. distance between the superconductor and permanent magnet for solid-state sintered YBCO (0), melt-processed YBCO (Δ), and melt-processed YBCO + 211 ( ).

Figure 4: Photograph showing large single crystal region of YBCO obtained by melt-processing YBCO + Pt using Sm-123 seed.

Figure 5: Optical micrograph of melt-processed YBCO + Pt using Sm-123 seed.

Figure 6: Levitation force vs. distance for melt-processed YBCO + Pt using Sm-123 seed.

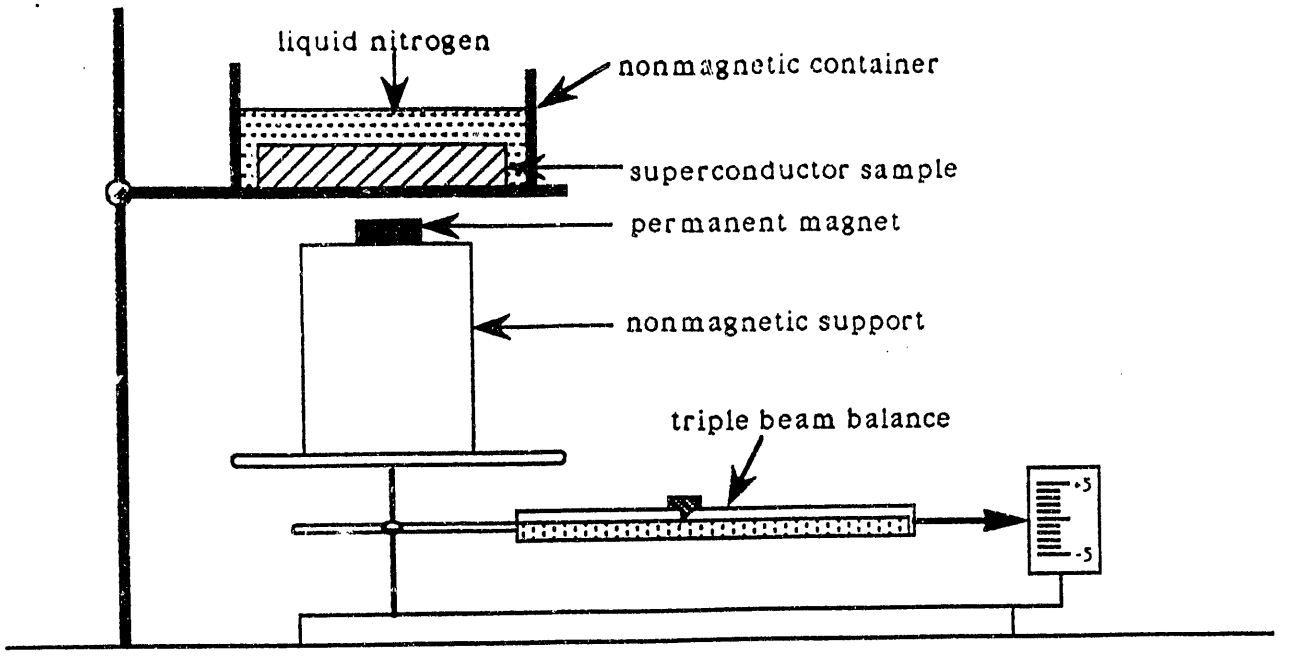
liquid nitrogen
nonmagnetic container
superconductor sample
permanent magnet
nonmagnetic support
triple beam balance
+5
-5

Figure 1

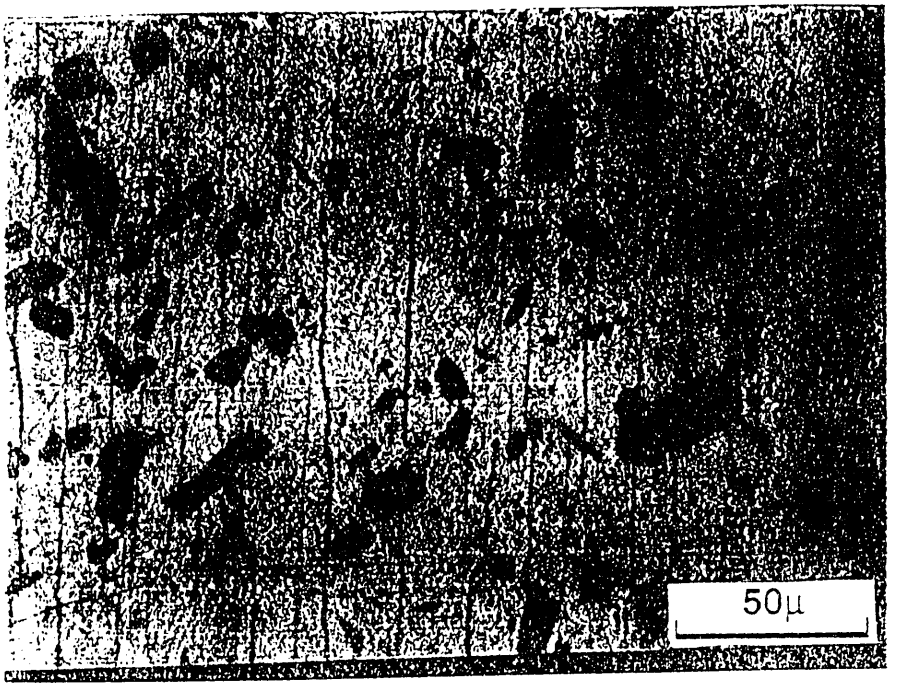

(a)

(b)

Figure 1

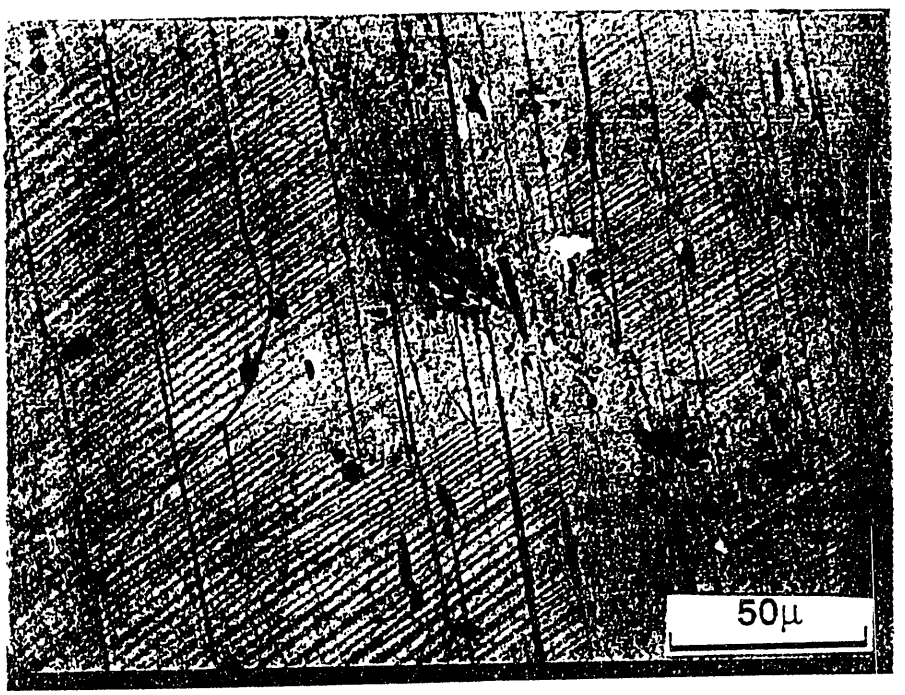

(c)

Figure 2

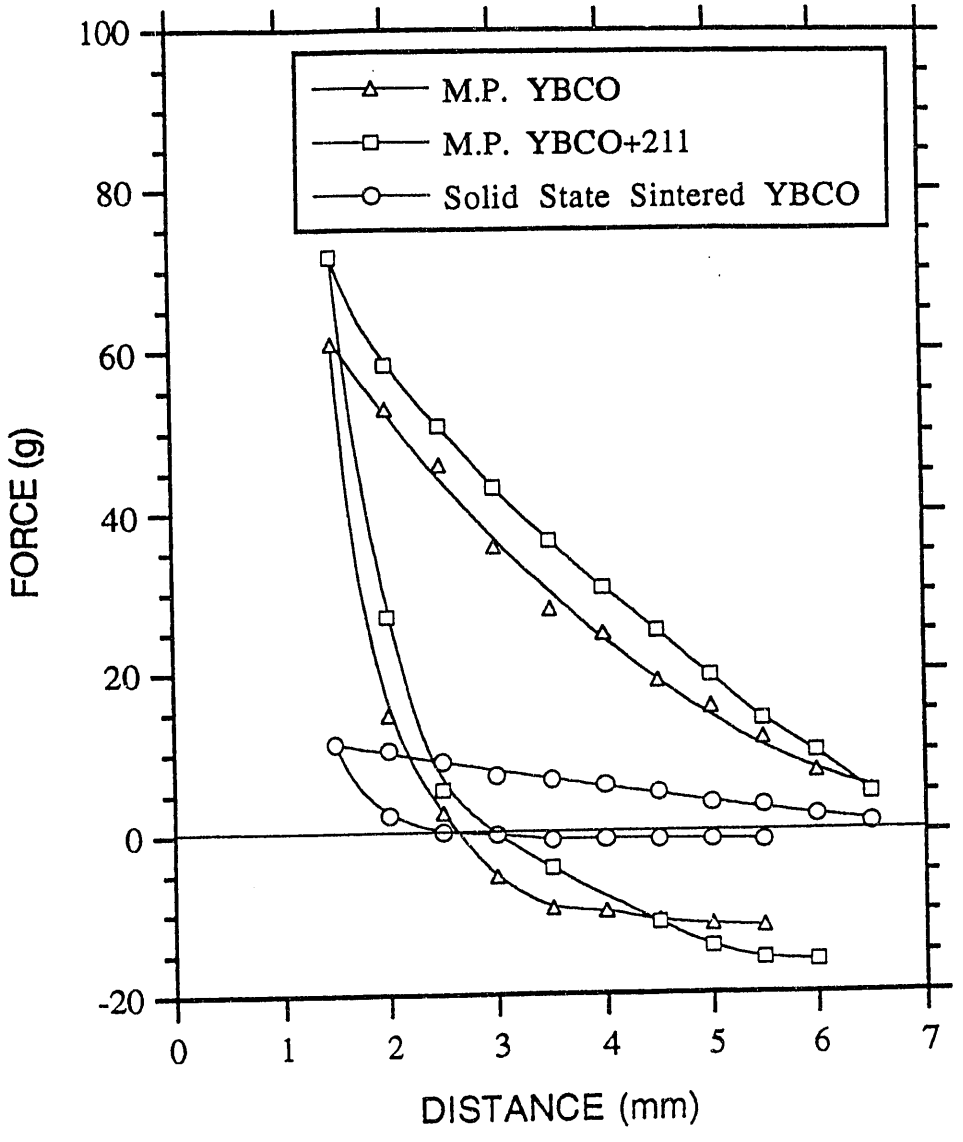
M.P. YBCO
M.P. YBCO+211
Solid State Sintered YBCO
FORCE (g)
DISTANCE (mm)
100
80
60
40
20
0
-20
0
1
2
3
4
5
6
7

Figure 3

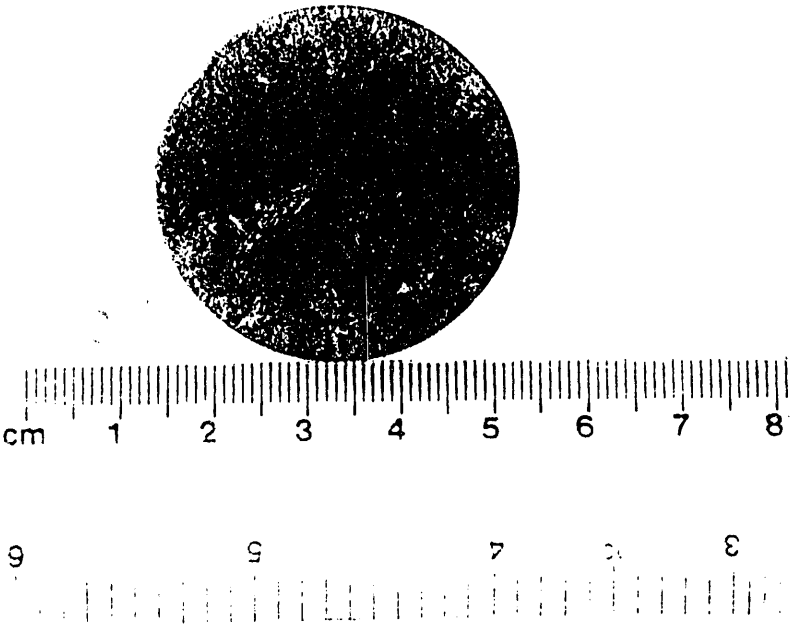

Figure 4

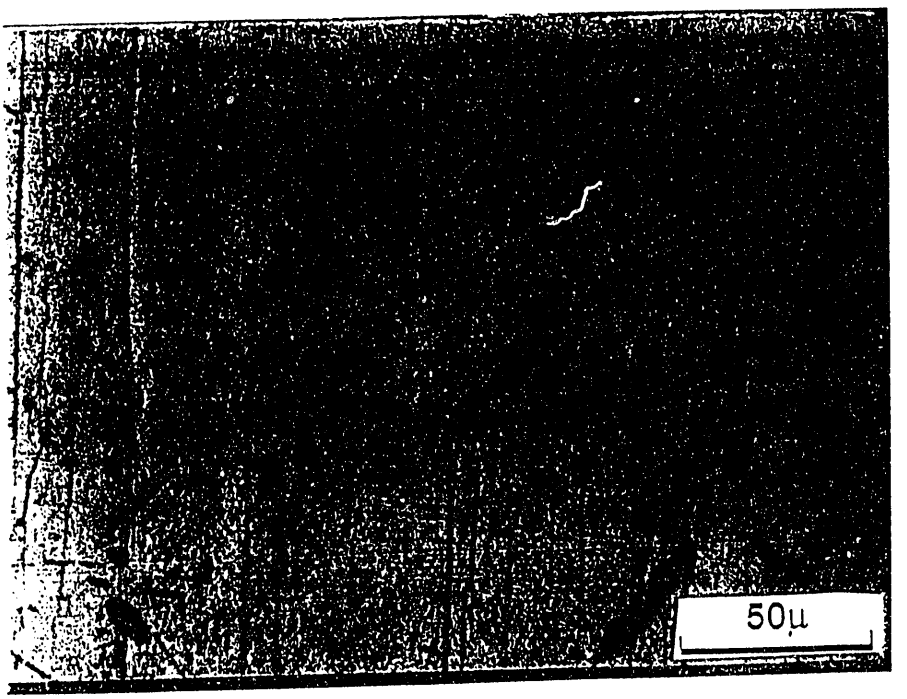

Figure 5

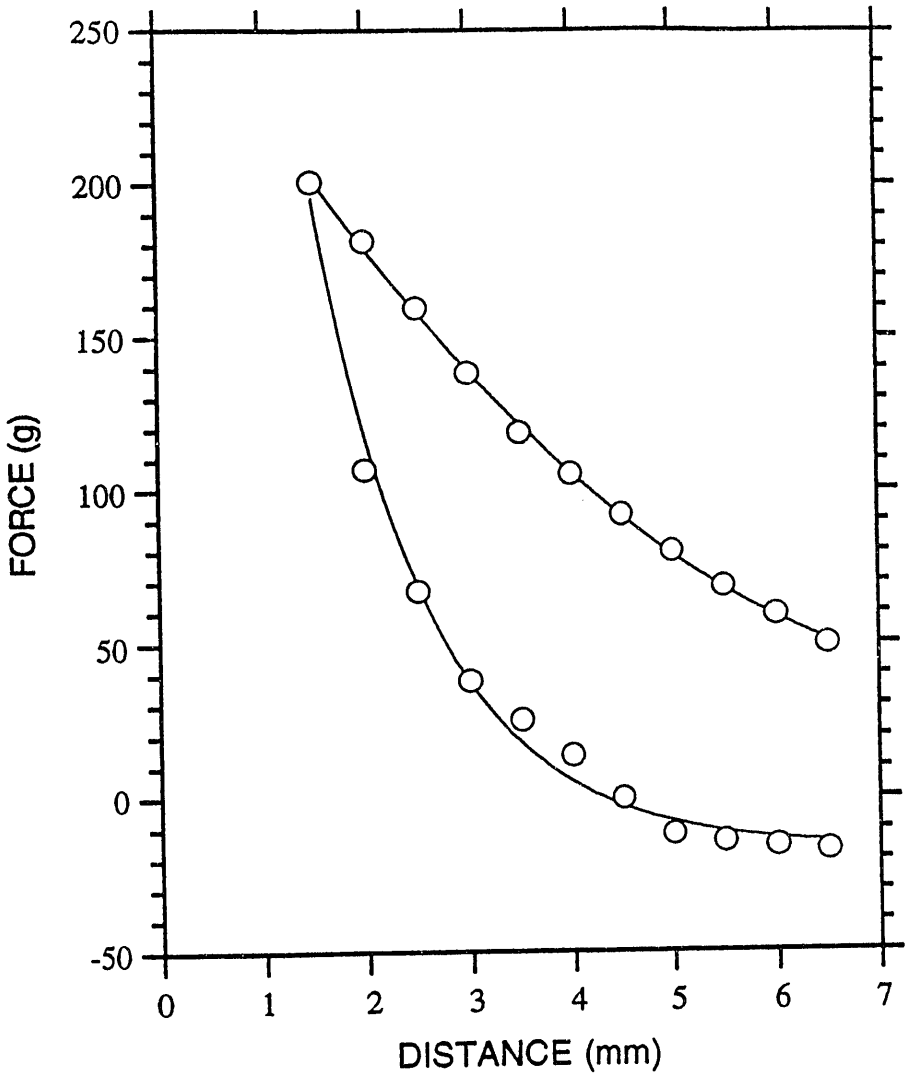

Figure 6

END

DATE
FILMED
6/11/93